Progress in Understanding Radio Emission from Solar Flares: Observations with the Nobeyama Radioheliograph 1999-2004

T. S. Bastian*
National Radio Astronomy Observatory
tbastian@nrao.edu

Abstract

Studies of solar flares based on observations by the Nobeyama Radioheliograph and related instruments such as the Owens Valley Solar Array, the Nançay Radioheliograph, and the Solar Submillimeter Telescope, as well as supporting instruments such as the RHESSI, TRACE, and SOHO missions, are reviewed for the period 1999-2004. Work on the classification of solar radio bursts is briefly discussed. Recent observational work on loop-top radio sources and rapidly propagating emission signatures is summarized and its interpretation in terms of electron anisotropies is described. Possible acceleration processes yielding such anisotropies are also briefly discussed. Recent work on electron acceleration and transport in a relatively dense plasma environment is summarized. Finally, recent work at millimeter and submillimeter wavelengths is described.

Key words: Sun: flares – Sun: radio radiation – Sun: X-rays, gamma rays

1. Introduction

The pursuit of understanding the physics of solar flares is a complex and multi-faceted affair. In order to piece the parts of a puzzle together observations across the electromagnetic spectrum are required, as well as insights and motivation gained through theory and modeling. Access to key pieces of the puzzle are provided by radio spectroscopic and imaging observations, which allow observers to image thermal and nonthermal electron emissions in the flaring source. Centimeter, millimeter, and submillimeter wavelength emissions are particularly important as probes of the most energetic electrons released in a flare. The Nobeyama Radioheliograph (NoRH) has therefore played a central role in extending our understanding of basic processes in solar flares and in uncovering new phenomena that occur during flares.

This review summarizes recent progress in understanding physical processes in solar flares based on radio observations. The emphasis is on observations made by the NoRH and by other radio observatories since the last Nobeyama Symposium in 1998 (Bastian et al. 1999). There have been two major observational developments during this time. First, beginning in May 1998, high resolution imaging in extreme ultraviolet (EUV) wavelengths by the Transition Region and Coronal Explorer (TRACE) became available and has played an important role in joint radio/EUV studies of flares (e.g., White, this proceedings). Second, beginning in February 2002, the Ramaty High Energy Spectroscopic Solar Imager (RHESSI) has provided high resolution spectroscopic imaging of hard X-ray (HXR) emission from flares and microflares (see Hudson, this proceedings). The contributions of both missions are reflected in the work presented in this proceedings.

More than half the papers presented in this proceedings are devoted to aspects of flares and particle acceleration and provide a good sample of progress in these areas. The magnetic evolution of flare-producing active regions is discussed by Pohjolainen and by Hori et al.; properties of energetic electrons in flares is discussed in papers by Nakajima et al., Takasaki et al, and Masuda; electron acceleration and transport processes are discussed by Melnikov and by Tanuma, with fast propagating radio signatures discussed by Shibasaki and by Hori et al.; gyrosynchrotron emission from anisotropic electron distributions are discussed by Fleishman; diagnostics of magnetic fields in flares are discussed by Huang; pulsation events and their interpretation are discussed by Kumio et al., Stepanov et al., and Asai; microflares are discussed by Kundu et al.; spatial and temporal fine structures are discussed by Altyntsev et al.; recent efforts to model microwave emission from flares are described by Nindos.

In the following, I provide a broad overview of several topics touched on in these proceedings and elsewhere in the literature. The overview is necessarily topical in nature but reflects those areas where I believe new phenomena have been uncovered and/or new insights have been gained into the flare phenomenon. I begin with recent work on the classification of radio bursts in §2. In §3 I discuss electron acceleration and transport, including the trap plus precipitation model, electron anisotropies, loop-top electron acceleration, and possible signatures of streaming electrons. In §4 I discuss plasma environments in which flares can occur, and in §5 I summarize recent work on millimeter and submillimeter observations of flares. I conclude in §6.

* The National Radio Astronomy Observatory is a facility of the National Science Foundation operated under cooperative agreement by Associated Universities, Inc.

2. The Spectral Taxonomy of Radio Bursts

It is worth beginning with a reminder of why observations at centimeter wavelengths (cm-λ) are important to studies of the flare phenomenon. It has been known since the 1960s (see, e.g., Kundu 1965 for a review of early work) that cm-λ emission is intimately related to HXR emission and that both serve as powerful tools for characterizing the population of electrons that often carry the bulk of the energy released in a flare. As such, they offer unique diagnostic of magnetic energy release, electron acceleration, and electron transport processes. Yet radio emission occurs over a much broader range than cm-λ. What is the importance of cm-λ emission relative to longer-wavelength (decimeter- and meter- wavelengths)? It has been known for many years (Giudice & Castelli 1975) that radio bursts are composed of multiple spectral components, classified as G, C, and A components according to whether the flux density decreased with frequency, showed a spectral maximum, or increased with frequency, respectively. It was found that pure C components accounted for a little more than half of the events observed (54%), while pure G and composite GC events accounted for 19% and 21% of the total, respectively. Of the remainder, A components accounted for only 1% of the total. Roughly 5% were classified as complex, or type M, for "miscellaneous".

An update to the work by Giudice & Castelli, who studied nine fixed frequencies between 245 MHz and 35 GHz has been performed by Nita et al. (2004), using the Owens Valley Solar Array (OVSA) between 1-18 GHz. While the OVSA study has narrower frequency coverage, it has frequency resolution of a few percent. Nita et al. classified bursts somewhat differently than Giudice & Castelli, designating bursts as type C (cm-λ), type D (cm-λ), or type CD. In contrast to Giudice & Castelli, Nita et al. find that 80% of their sample of 412 OVSA events are pure C, whereas only 5% are pure D and 15% are CD. Of the composite CD events, 12% had peak flux densities < 100 SFU, 19% had peak flux densities between 100-1000 SFU, and 60% had peak flux densities > 1000 SFU. That is, composite events tend to be large events. Interestingly, Castelli et al. (1967) first drew attention to the correlation between large GC (or type "U") events and major proton events as manifested by polar cap absorption events at 30 MHz.

To summarize, a modern classification of dm-λ to cm-λ radio bursts shows that the majority (80%) are pure C type; cm-λ studies of flares therefore provide access to the most common manifestation of radio emission from flares. A critical class of flares are those of type CD or GC that include dm-λ and/or m-λ emission. These tend to be the largest flares and are associated with solar energetic particle events. Type G or D emission has a detailed taxonomy of its own (e.g., radio bursts of type II, III, and IV) but these topics, albeit fascinating, lie outside the scope of this review. However, at the opposite end of the radio spectrum we discuss recent work on high frequency bursts at mm-λ and submm-λ in §6.

3. Electron Injection and Transport

Emissions from energetic electrons at X-ray and radio wavelengths have played a central role in making progress toward an understanding of the flare phenomenon. At cm-λ, energetic electrons emit via the well-understood gyrosynchrotron mechanism whenever and wherever energetic electrons interact with magnetic fields. Observations of gyrosynchrotron emission are therefore ideally suited as a probe of electron acceleration and transport processes in flares. However, effective exploitation of cm-λ emission depends on appropriate instrumentation. As a solar-dedicated imaging instrument operating at 17 and 34 GHz, the NoRH provided an important step in this direction and has made several important contributions to revealing new phenomena relevant to electron acceleration and transport. After summarizing a framework in which many features of HXR and cm-λ observations can be understood, recent developments are described.

3.1. TTP/DP Model

Beginning with Melrose & Brown (1976) the so-called "trap plus precipitation" (TPP) model has enjoyed some success in explaining various features of HXR and cm-λ observations in many flares. The TPP model is based on the idea that coronal magnetic loops serve naturally as magnetic traps. An electron in a uniform magnetic field and with velocity components parallel and perpendicular to the magnetic field vector will follow a helical trajectory with a pitch angle $\alpha = 3Dtan^{-1}(v_\perp/v_\parallel)$. In coronal magnetic loops the magnetic field is stronger at its footpoints than at its looptop and the magnetic field therefore converges as it nears the Sun. Since the first adiabatic invariant $\mu = p_\perp^2/2B \propto v_\perp^2/B$ is conserved, $v_\perp$ increases and $v_\parallel$ decreases as B increases. The pitch angle α therefore increases as an electron propagates toward the chromosphere. One of two things then happens: if the electron propagates close enough to the Sun it penetrates the chromosphere and loses its energy to Coulomb collisions in the high-density environment and is lost from the trap, a process called electron precipitation. Alternatively, if the electron's pitch angle reaches 90° before it suffers significant energy loss due to collisions, it mirrors and remains in the coronal magnetic loop. Let $\alpha_\circ$ represent the initial pitch angle of an electron injected into the loop. The loss cone is defined by the angle $\alpha_{LC} = 3D\sin^{-1}[(B_\circ/B_p)^{1/2}]$, where $B_\circ$ is the magnetic field strength where the electron is injected and B_p is its value at the height where it precipitates from the loop. Electrons with pitch angles $\alpha_\circ < \alpha_{LC}$ are in the loss cone and therefore directly precipitate from the loop whereas electrons with $\alpha_\circ > \alpha_{LC}$ mirror at the foot points and remain trapped in the loop until some physical process scatters them into the loss cone and/or they lose their energy and are thermalized. Several mechanisms cause electrons to scatter into the loss cone. Coulomb collisions between electrons and electrons, and electrons and ions, are omnipresent and establish the maximum lifetime of an electron in the trap. However, other scattering mechanisms – e.g., wave-particle interac-

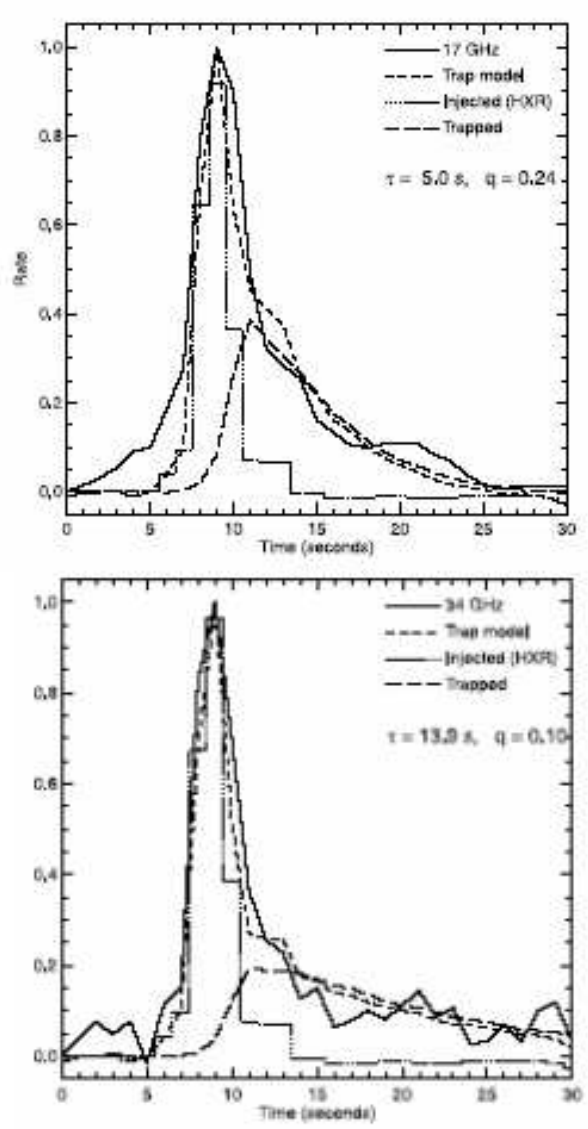

Fig. 1. Observations of the 1998 Jun 13 flare. Light curves are shown for the 17 and 34 GHz emission, and relative count rates for the *Yohkoh* HXT 53-93 keV channel (M2). The HXR profile is used as a proxy for the electron injection rate. The data are compared with a trapping model. The long-dashed curves represent emission from the trapped electrons. After Fig. 7 in Kundu et al. (2001).

tions (Bespalov et al. 1987)– may cause strong- or diffusive pitch-angle scattering on much shorter time scales and therefore dominate electron transport. In the simplest version of the TPP model, however, Coulomb collisions dominate.

Electron injection and transport in the context HXR emission and the TPP model have been studied by numerous authors: e.g., Emslie et al. 1979, MacKinnon et al. 1983, Vilmer et al. 1986, Hulot et al. 1989, Alexander 1990, McClements 1990, Bruggman et al. 1994, Aschwanden et al. 1997, Alexander & Metcalf 2002, to name just a few. For electrons with energies $< 160keV$, the Coulomb collision frequency $\nu_C \propto n_{th}E^{-3/2}$. Since more energetic electrons suffer fewer collisions than less-energetic electrons, they have longer life times in the trap. In this way, the distinctive delay structure of energetic photon emissions in HXR, and in high frequency radio emission at cm-λ, can be understood as well as the relative timing between electronic and ionic emissions (e.g., Hulot et al. 1989, 1992). Moreover, the background density in the trap n_{th} can be inferred by detailed analysis of HXR or radio delays as a function of energy (Aschwanden et al. 1997) or frequency (Lee et al. 2000, Lee & Gary 2000). A recent example of NoRH observations of a simple impulsive flare that shows clear evidence of electron trapping at 17 and 34 GHz is shown in Fig. 1 (from Kundu et al. 2001a).

Aschwanden et al. (1997, 1998a,b) pointed out that for an injection of electrons into the magnetic trap, some fraction will have pitch angles such that they are in the loss cone and they directly precipitate (DP) from the trap. The fraction of injected electrons that directly precipitate from the trap depends on the magnetic mirror ratio $R = 3DB_p/B_\circ$. This modification of the TPP model is referred to as the "trap plus precipitation/direct precipitation" (TPP/DP) model (Fig. 2). The DP component is of great interest because it reflects the energy distribution function of the injected electrons, unmodified by transport effects other than time-of-flight dispersion from the injection site to the precipitation point, assuming no evolution of the injection spectrum during an injection time (Brown et al. 1998). The TPP/DP model represents an interesting deconvolution problem. In many cases, the coronal (thin target) contribution to the HXR emission is negligible and the emission is dominated by thick-target bremsstrahlung emission by electrons precipitating from the magnetic trap. Hence, the HXR emission is dominated by footpoint emission composed of DP electrons and those that have been trapped for a time before precipitating. In other words, HXR emission is generally only sensitive to precipitating electrons. In contrast, microwave emission is sensitive to the entire distribution of electrons (both trapped and DP components). However, the trapped component is expected to dominate the emission at a given frequency because the number density of trapped electrons represents a time-integral of the injection function over a trapping time whereas the DP component is promptly lost from the trap.

Gyrosynchrotron and HXR radiation are thus highly complementary. Unfortunately, this complementarity has been difficult to exploit in practice, primarily because of limitations in available instrumentation. Both spectral regimes require the means to perform time-resolved broadband imaging spectroscopy. While RHESSI indeed has the means to do this, it is not yet possible to do so at radio wavelengths. Instead, observers have often been forced to rely on total flux measurements at fixed frequencies (NoRP, Berne) and/or time-resolved imaging at only one or two frequencies (NoRH), or low-resolution imaging spectroscopy (OVSA). Nevertheless, recent observations have shown that while the TPP or TPP/DP models provide a useful framework for interpreting the observations,

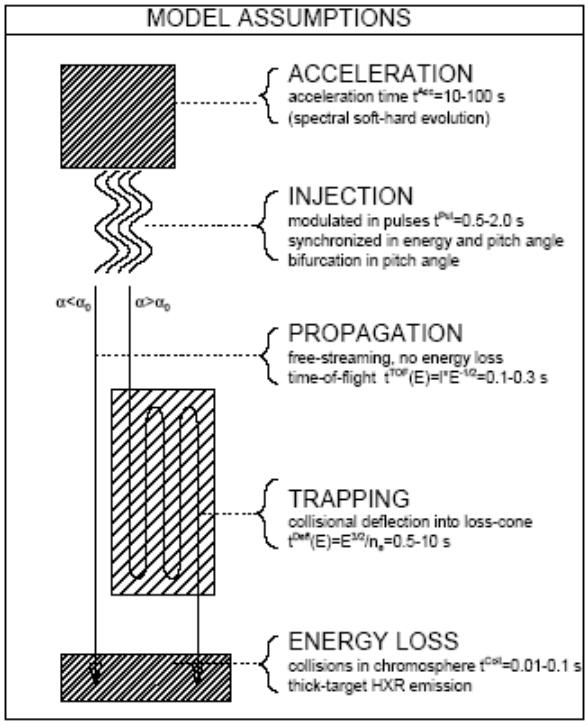

Fig. 2. Schematic of the TPP/DP model where upon injection, those electrons with pitch angles within the loss cone directly precipitate, whereas those electrons with pitch angles outside the loss cone will remain trapped until scattered into the loss cone. From Aschwanden (1998).

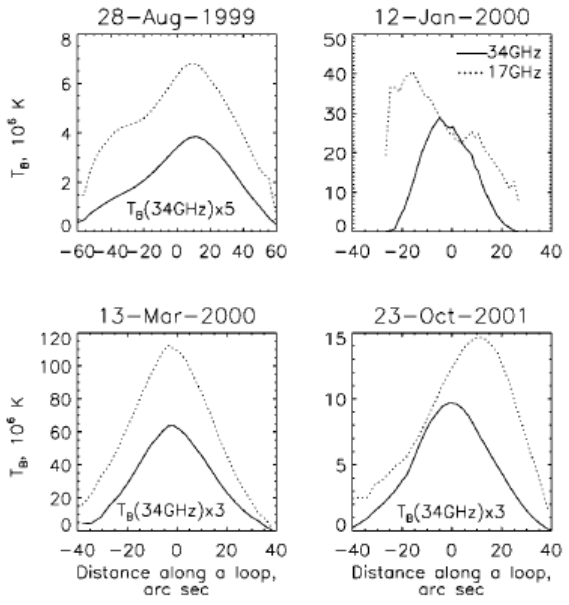

Fig. 3. Examples of loop-top sources. Each panel shows the variation of brightness at 17 and 34 GHz along the length of a flaring loop. From Melnikov et al. (2002).

they are by no means the full story. For the remainder of this section, I touch on examples of recent flare observations that show evidence for strong electron anisotropies and their possible causes, as well as observations that may show evidence for streaming, or beamed, electrons.

3.2. Electron Anisotropy

For an isotropic distribution of energetic electrons in a coronal magnetic loop, the morphology of the gyrosynchrotron source is strongly frequency dependent. Bastian et al. (1998) show that at high frequencies, the source is footpoint-dominated whereas at low frequencies, the source can be optically thick and the maximum brightness is found at the loop top in such cases. An important development in recent years is the identification of "loop top" sources in flares observed at high frequencies by the NoRH. While loop top sources had been suggested long ago (e.g., Marsh & Hurford (1982) and references therein) on the basis of early observations made by the Very Large Array, recent OVSA and NoRH observations have stimulated renewed interest in the loop top sources and their underlying cause or causes.

White et al. present 17 and 34 GHz observations of the M1.6 flare at S23E60 on 1999 May 29. The microwave emission was optically thin and, in the early phase of the flare, originated in the loop footpoints or loop legs. However, as the flare proceeded the source evolved to a complete loop morphology dominated by a loop top source at both 17 and 34 GHz, a morphology that could not be fit by gyrosynchrotron emission from a simple isotropic electron distribution function. Melnikov et al. (2002) present a sample of four flares, each of which shows clear evidence for loop top sources at 17 and 34 GHz (Fig. 3). The authors find that the observed emission is consistent with an anisotropic distribution of energetic electrons near the loop top, the sense of the anisotropy such that the electron distribution is strongly peaked perpendicular to the magnetic field. Melnikov et al. conclude that the anisotropy likely reflects that of the injected electrons and therefore yields insight into the electron acceleration/injection mechanism.

Lee et al. (2000) studied two flares, A and B, that occurred in close succession on 1993 June 3 with NoRH and OVSA. The microwave emission of flare A was significantly greater in intensity and duration than that of flare B. In contrast, the SXR emission from flare A (GOES C2.8) was significantly less than that of flare B (GOES M1). The spectral evolution of flare A suggested that electron energy loss was dominated by Coulomb collisions and that the background density in the magnetic trap was relatively low (5×10^9 cm^{-3}) whereas the background density inferred for flare B was substantially higher (8×10^{10} cm^{-3}). In a second study, Lee & Gary 2000 explored the spectral evolution of the microwave spectrum of flre A in the context of the TPP model under the assumption that the evolution was the result of electron transport effects and was not a function of electron acceleration or injection. Included in the formulation was an anisotropic electron distribution function. Fitting to the (optically thin) total power spectra, Lee & Gary find that the best-fit model indeed required an anisotropic distribution that

was strongly peaked (angular width $\approx 30°$) perpendicular to the magnetic field.

Several lines of observational evidence, based on imaging and spectroscopy of microwave sources, suggest that anisotropic electron populations that are located near the tops of flaring magnetic loops and are strongly peaked perpendicular to the magnetic field. In order to fully characterize the phenomenon, the incidence and circumstances of loop top sources must be determined and their circumstances explored using suitably selected statistical samples. In addition to the imaging domain, the spectral domain can be more fully exploited to explore anisotropic electron distribution functions. Fleishman & Melnikov (2003a,b) have computed gyrosynchrotron emission spectra expected from various anisotropic electron distribution functions and find that the intensity, spectral index, and source polarization are all sensitive to the degree and type of anisotropy. Hence, polarization spectroscopy could be an important tool for probing electron anisotropies in flares.

3.3. Loop-top Acceleration

Important questions follow from the conclusion that anisotropic electron distributions are produced by some flares near the tops of coronal magnetic loops: what physical process or processes produce such distributions and what do they tell us about electron acceleration, injection, and transport? These questions have not yet been answered in detail but preliminary explorations have been made into acceleration mechanisms that may be operative near coronal loop tops that would result in electron distributions that are strongly peaked perpendicular to the magnetic field.

Somov & Kosugi (1997) proposed that collapsing magnetic traps may play a role as a secondary electron acceleration mechanism in flares. In the "standard" flare scenario, magnetic reconnection takes place in a current sheet above flare loops (e.g., Forbes & Priest 2000) in a cusp configuration. Reconnected field lines relax in succession from the cusp-like topology to a more-nearly force-free configuration (Fig. 4). Karlický & Kosugi (2004) modeled this idea numerically, including the effects of Coulomb collisions, and found that electrons could be betatron-accelerated to high energies and that highly anisotropic distribution functions resulted at the loop top. It is worth mentioning that, to overcome energy losses to Coulomb collisions, effective acceleration of electrons via the collapsing magnetic trap model requires the injection of electrons that have already been accelerated to an energy above some threshold energy. Pre-acceleration may plausibly occur in the current sheet via DC electric fields.

Qiu et al. (2004) present OVSA and *Yohkoh* HXT observations of the X-class flare observed on 2001 Apr 6, which is characterized by an impulsive and gradual phase. The gradual phase shows evidence for footpoint separation and continuing thick target HXR emission, implying continuing electron acceleration during the gradual phase. Qiu et al. propose that, in this example, the collapsing trap model is a viable acceleration mechanism.

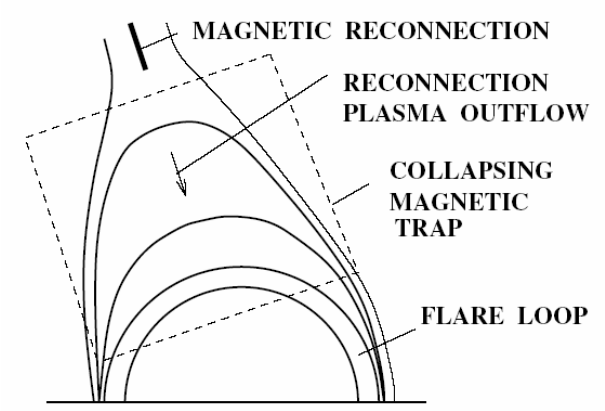

Fig. 4. Schematic of the collapsing magnetic trap. From Karlický & Kosugi (2004).

Aschwanden (2004) explores a similar "dynamic trap" model to account for the apparent synchronization of pulsed particle injection as inferred from time-of-flight measurements of electrons using in HXR observations. Noting that the loss cone would increase as the magnetic field relaxed from a cusp-like to force-free configuration, Aschwanden suggests electrons could be injected into the trap in a largely energy-independent manner.

While a great deal of both observational and theoretical work remains in order to understand the role that anisotropic electrons play in the flare phenomenon, it is interesting to note that magnetic trap models – TPP, TPP/DP, and now, collapsing or dynamic magnetic traps – continue to play a fruitful role.

3.4. Fast Electron Propagation

A scientific goal of the NoRH was to resolve in time electron propagation effects in flares and related phenomena. One such example is that of a collimated ejection of nonthermal electrons in association with a flare and Hα surge, reported by Nakajima & Yokoyama (2002). The collimated jet moved upward with an apparent speed of ≈ 3000 km s^{-1}. A second intriguing example was reported by Yokoyama et al. (2002), who observed the GOES M2.8 flare of 1999 Aug 28. The flare was analyzed in a high cadence imaging mode at 17 and 34 GHz, where 10 images per second were produced. At least two propagating features were measured in the high cadence images. One appeared to propagate at a speed > 6000 km s^{-1} whereas another appeared to propagate at 90000 km s^{-1}; i.e., at $0.3c$.

The authors interpret the rapidly propagating signal in terms of fast electrons streaming from one end of the magnetic loop to the other. A problem raised by this interpretation is that if the speed of the emitting electrons is taken to be that of the propagating gyrosynchrotron emission, the energy of the emitting electrons is only 23 keV. This is far less than the expected energy of electrons responsible for the 17 GHz emission: the authors argue that the magnetic field strength in the source must be of order 200-400 G, implying the energy of the emitting

electrons is of order 1 MeV. The speed of 1 MeV electrons is nearly that of light. The authors suggest the discrepancy might be resolved if the fast electrons are injected into the source with a relatively large pitch angle ($\approx 70°$). The signal with a lower apparent propagation speed may be consistent with the local Alfvén speed or, perhaps, with the propagation of a "turbulent mirror".

4. Dense and Cool Flares

The plasma density in flaring loops has been studied for many years using SXR and EUV observations. These studies have produced density estimates ranging from 10^{10} cm^{-3} to more than 10^{12} cm^{-3} (e.g., Doschek 1990). Aschwanden et al. (1997) have considered radio and SXR diagnostics of the electron number density in flaring loops. In particular, in an analysis of 14 different flares, they compare electron number densities derived from *Yohkoh* SXT observations with those inferred from dm-λ radio bursts and find that the values inferred depend on the time and place the measurement is made. Using type IIIdm and reverse-slope dm-λ radio bursts, densities of 6×10^8 cm^{-3} to 10^{10} cm^{-3} are inferred in the electron acceleration region. The accelerated electron are stopped in the chromosphere, liberating their energy and driving so-called chromospheric evaporation. Again, using dm-λ radio bursts, Aschwanden & Benz find densities of 10^9 cm^{-3} to 5×10^{10} cm^{-3} at the evaporation front, presumably reflecting the pre-flare loop density; they find densities a factor of 3.6 higher (i.e., 4×10^{10} cm^{-3} to 2×10^{11} cm^{-3}) behind the fronts. Finally, the densities inferred for "filled" loops based on SXR measurements is 2×10^{10} to 2.5×10^{11}. Therefore, while large densities are expected following main-phase energy release and the evaporation it produces, pre-flare loop densities do not appear to be large.

Nevertheless, in some cases, even pre-flare loop densities can be significant. Veronig & Brown (2004) report two examples of a new class of HXR source where the corona is so dense that it is collisionally thick to electrons with energies up to 50 keV, with chromospheric evaporation dominated by energy deposition via conduction rather than electron precipitation. Initial loop densities in excess of 10^{11} cm^{-3} are inferred. It is interesting to note that high plasma densities and temperatures can yield a high plasma β. Shibasaki (2001) has recently considered the implications of high-β plasma environments for flaring and has suggested such environments may be unstable to the "ballooning instability".

More recently, Bastian, Fleishman, & Gary (2006) have analyzed an example of a flare observed on 24 Oct 2001 by the NoRH, NoRP, OVSA, TRACE, and *Yohkoh*. This flare is similar to that observed by White et al. (1992), described as an "impulse response" event by Hudson & Ryan (1995). These events are characterized by a steep low-frequency spectral cutoffs indicative of a high ambient density which causes both Razin suppression and free-free absorption below ~ 10 GHz. The event reported by White et al. showed no frequency-dependent delays in the flux maximum, in contrast to expectations based on the TPP or TPP/DP model. The event analyzed by Bastian et al. shows delays that show a frequency dependence that is opposite to that expected for the TPP or TPP/DP model. A detailed analysis of the event resulted in the following scenario: that the radio source initially comprised a cool ($\sim 2 \times 10^5$ K), dense (10^{11} cm^{-3}) plasma permeated by a magnetic field of order 165 G. The radio emission and its spectral shape and evolution result from an injection of fast electrons into the dense ambient plasma. Due to a large magnetic mirror ratio neither electron precipitation, nor thermal conduction, produced significant chromospheric evaporation. Therefore, the density of the flaring loop did not change significantly during the course of the flare. Importantly, however, energy was deposited in the loop via collisions and/or turbulent heating that yielded a significant increase in plasma temperature. The temperature increase led to decreased free-free absorption and could account for the inverse delay structure of the event.

To conclude this section, both radio and HXR techniques have revealed new types of environments in which energy release and electron acceleration appears to occur. The extreme nature of these environments may lead to new insights regarding the energy release mechanism and/or particle acceleration and transport.

5. Submillimeter Emission from Flares

With the advent of the Solar Submillimeter Telescope (SST) at El Leoncito in the Argentine Andes (Kaufmann et al. 2000), and the Köln Observatory for Submillimeter and Millimeter Astronomy (KOSMA) near Zermat, Switzerland (Lüthi et al. 2004), a new spectral window has opened at mm- and submm-λ wavelengths. The SST is a 1.5 m telescope that operates at 212 and 405 GHz while KOSMA is a 3 m telescope that operates at 230 and 345 GHz. Emissions at these frequencies probe relativistic electrons accelerated in flares. It has been known for some time that a different population of energetic electrons may be involved in the production of mm-λ radiation, at least for some flares. Observations with the Berkeley, Maryland, Illinois Array (BIMA) suggested that the electron energy distribution function flattens toward higher energies (e.g., Kundu et al. 1994). For example, Trottet et al. (1998) present HXR and γ-ray spectroscopy of flares wherein the cm-λ/mm-λ emission appears to be associated with electrons with energies of 0.4-0.7 Mev, which have a flatter spectrum than lower energy electrons. Trottet et al. (2002) report the first observations of a flare above 200 GHz. The observations, made jointly with the SST and OVSA, showed an impulsive spike produced by synchrotron emission from relativistic electrons with energies of 10-15 MeV, and an extended phase that was mostly due to thermal free-free emission=2E They show that in this case, too, the 212 GHz impulsive emission appears to be a due to electrons with a rather hard energy spectrum. A number of additional new and intriguing observations have been reported from the SST and KOSMA.

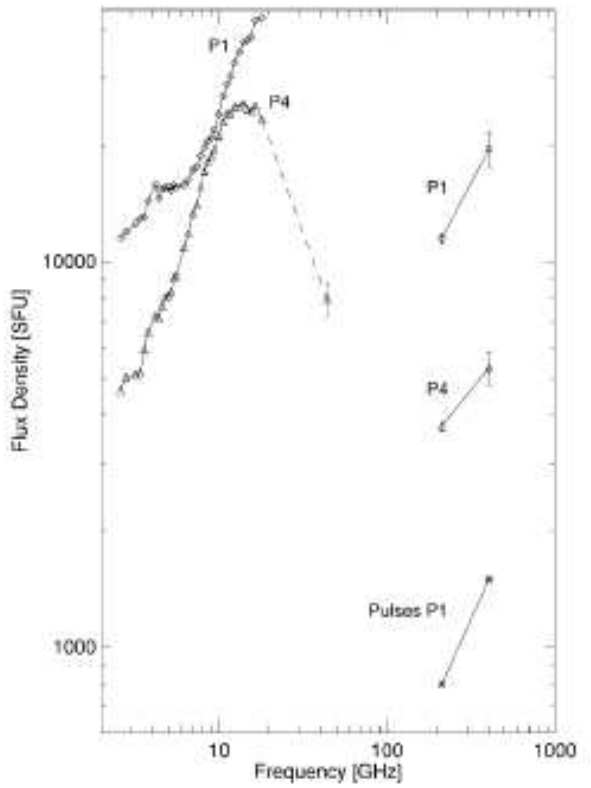

Fig. 5. Spectra of the 2003 Nov 4 flare from cm-λ to submm-λ. Note that while the cm-λ emission appears to be consistent with gyrosynchrotron emission, the submm-λ spectral component is inverted. From Kaufmann et al. (2004).

Kaufmann et al. (2001, 2002) report SST and OVSA observations of the X1.1 on 22 Mar 2000 and the X5.6 flare on 6 Apr 2001. A new and curious feature of the submm-λ emission is the presence of sub-pulses or spikes of radiation, with amplitudes of 5-10% and a recurrence rate of ≈ 50 per minute. Raulin et al. (2003) studied the spike phenomenon in the X5.3 flare of 25 Aug 2001, demonstrating that spikes observed at 212 and 405 GHz are correlated and that the pulse rate is correlated with the overall flux of the event. Raulin et al. suggest that the spikes are intimately related to primary energy release. A second study of the same flare (Raulin et al. 2004) suggests that the energy requirements of the event were extreme, requiring that $\approx 5 \times 10^{36}$ electrons must be accelerated to energies > 20 keV each second in a source with a magnetic field strength > 1 kG!

A second intriguing discovery was reported by Kaufmann et al. (2004) in which the presence of an inverted high frequency spectral component is reported (Fig. 4). In particular, the flare of 4 Nov 2003 displays a spectrum that *increases* between 212 and 405 GHz, in stark contrast to the flat or strongly decreasing spectrum expected for optically thin thermal free-free emission or nonthermal gyrosynchrotron emission, respectively. Using observations from KOSMA and the Berne polarimeters, Lüthi et al. (2004) present an analysis of the flare of the GOES X17.2 flare that occurred on 28 Oct 2003. Here, too, an inverted spectrum is seen from 230 to 345 GHz. The cause of the inverted spectral component is presently unknown. Among the possibilities are emission from optically thick thermal or nonthermal components, positron emission (Lingenfelter & Ramaty 1967), inverse Compton radiation (Kaufmann et al. 1986), or another mechanism.

6. Summary and Conclusions

This brief review has summarized progress on several fronts related to microwave observations of solar flares, with particular emphasis on observations from the NoRH, and joint observations made by the NoRH and HXR instrumentation such as *Yohkoh* and RHESSI, as well as examples of those made jointly with TRACE. Microwave observations are well matched to the majority of solar flares, which produce gyrosynchrotron emission in this wavelength band.

While the TPP and TPP/DP models have provided a useful framework for understanding a number of aspects of both radio and HXR observations of flares, recent work has highlighted the presence of loop-top sources in flares. These are the result of highly anisotropic electron distributions, the distribution being strongly peaked perpendicular to the magnetic field. As a means of explaining such distributions, as well as the energy dependence of HXR pulse timing, dynamic or collapsing trap models have been considered. In addition to perpendicular anisotropies, it is possible that gyrosynchrotron emission from streaming or beamed electron distributions has been observed. It appears that energy release occurs in relatively dense, collisionally thick environments, as discovered by RHESSI. However, NoRH and NoRP observations have shown that energy release in cool and dense environments is also possible. Finally, recent work at submm-λ has revealed the presence of a new spectral component during flares. The origin of this component is presently unknown.

To conclude, while progress on some outstanding problems has been made, new and intriguing observational phenomena have been discovered. Future work requires joint observations across the electromagnetic spectrum as well as further progress in developing next-generation radioheliographs (e.g., the Frequency Agile Solar Radiotelescope) to supplement and to build upon the excellent work done with the NoRH.

References

Aschwanden, M. J. 1998, ApJ 502, 455
Aschwanden, M. J. 2004, ApJ 608, 554
Aschwanden, M., et al. 1997, ApJ 487, 936
Aschwanden, M. J., Schwartz, R. A., & Dennis, B. R. 1998, ApJ 502, 468
Alexander, D. 1990, A&A, 235, 431
Alexander, D., & Metcalf, T. R. 2002, Solar Phys., 210, 323
Bastian, T. S., Gopalswamy, N., & Shibasaki, K. (eds.) 1999, Solar Physics with Radio Observations, NRO Rep. No. 479
Bastian, T. S., Benz, A. O., & Gary, D. E. 1998, ARAA 36, 131

Bastian, T. S., Fleishman, G. F., & Gary, D. E. 2006, ApJ, submitted.
Bespalov, P. A., Zaitsev, V. V., & Stepanov, A. V. 1987, Solar Phys., 114, 127
Bruggmann, G., Vilmer, N., Klein, K.-L., Kane, S. 1994, Solar Phys. 149, 171
Castelli, J. P., Aarons, J., & Michael, G. A. 1967, JGR, 72, 5491
Emslie, A. G., McCaig, M. G., & Brown, J. C. 1979, Solar Phys., 63, 175
Fleishman, G. D., & Melnikov, V. F. 2003, ApJ 587, 823
Fleishman, G. D., & Melnikov, V. F. 2003, ApJ 584, 1071
Giudice, D. A., & Castelli, J. P. 1975, Sol. Phys. 44, 155
Hulot, E., Vilmer, N., & Trottet, G. 1989, A&A, 213, 383
Hulot, E., Vilmer, N., Chupp, E. L., Dennis, B. R., & Kane, S. R. 1992, A&A, 256, 273
Karlický M. & Kosugi, T. 2004, A&A 419, 1159
Kaufmann, P., Correia, E., Costa, J. E. R., Zodi Vaz, A. M. 1986, A&A 157, 11
Kaufmann, P., et al. 2000, in ASP Conf. Ser. 206, High Energy Solar Physics: Anticipating HESSI, ed. R. Ramaty & N. Mandshavidze (San Francisco: ASP), 318
Kaufmann, P., et al. 2001, ApJ 548, L95
Kaufmann, P., et al. 2002, ApJ 574, 1059
Kaufmann, P., et al. 2004, ApJ 603, L121
Kundu, M. R. 1965, Solar Radio Astronomy (New York: Interscience Publication)
i, K., & Sakurai, T. 2000, ApJ 545, 1084
133, 467
Kundu, M. R., White, S. M., Shibasaki, K., Sakurai, T., & Grechnev, V. V. 2001, ApJ 547, 1090
Lee, J., & Gary, D. E. 2000, ApJ 543, 457
Lee, J., Gary, D. E., & Shibasaki, K. 2000, ApJ 531, 1109
Lee, J., Gary, D. E., Qiu, J., & Gallagher, P. T. 2002, ApJ 572, 609
Lee, J., Bong, S.-C., & Hong, S. Y. 2003, JKAS, 36, 63
Lüthi, T., Lüdi, A., & Magun, A. 2004, A&A, 420, 361
Lingenfelter, R. E., & Ramaty, R. 1967, P&SS, 15, 1303
Marsh, K. A., & Hurford, G. J. 1982, ARAA, 20 497
McClements, K. G. 1990, A&A, 230, 213
Melrose, D. B., & Brown, J. C. 1976, MNRAS 176, 15
akajima, H., & Yokoyama, T. 2002, ApJ 570, L41
Nita, G. M., Gary, D. E., & Lee, J. 2004, ApJ 605, 528
Qiu, J., Lee, J., & Gary, D. E. 2004, ApJ 603, 335
Raulin, J.-P., et al. 2004, ApJ 592, 580
Raulin, J.-P., et al. 2004, Solar Phys. 223, 181
Shibasaki, K. 2001, ApJ, 557, 326
Somov, B., & Kosugi, T. 1997, ApJ 485, 859
Trottet, G., Chupp, E. L., Marschhaeuser, H., Pick, M., Soru-Escaut, I., Rieger, E., & Dunphy, P. P. 1994, A&A, 288, 647
Trottet, G., et al. 1998, A&A, 334, 1099
Trottet, G., et al. 2000, A&A, 356, 1067
Trottet, G., Raulin, J.-P., Kaufmann, P., Siarkowski, M., Klein, K.-L., & Gary, D. E. 2002, A&A, 381, 694
Veronig, A. M., & Brown, J. C. 2004, ApJ 603, L117
Vilmer, N., Trottet, G., & MacKinnon, A. L. 1986, A&A 156, 64
White, S. M., Kundu, M. R., Bastian, T. S., Gary, D. E., Gurford, G. J., Kucera, T., & Bieging, J. H. 1992, ApJ 284, 656
White, S. M., Kundu, M. R., Garaimov, V. I., Yokoyama, T., & Sato, J. 2002, ApJ 576, 505
White, S. M., Krucker, S., Shibasaki, K., Yokoyama, T., Shimojo, M., & Kundu, M. R. 2003, ApJ 595, L111
Yokoyama, T., Nakajima, H., Shibasaki, K., Melnikov, V. F., & Stepanov, A. V. 2002, ApJ 576, L87